Letter

Experimental storage of photonic polarization entanglement in a broadband loop-based quantum memory

C. J. Evans , C. M. Nunn , S. W. L. Cheng , J. D. Franson, and T. B. Pittman

Department of Physics, University of Maryland Baltimore County, Baltimore, Maryland 21250, USA

We experimentally study the ability of a broadband "loop-and-switch" type quantum memory device to store entanglement. We find that one active loop-based memory and one passive fiber delay line can be used to faithfully store two polarization-entangled photons and demonstrate a rudimentary entanglement distribution protocol. The entangled photons are produced by a conventional spontaneous parametric down-conversion source with center wavelengths at 780 nm and bandwidths of $\sim$10 THz, while the memory has an even wider operational bandwidth that is enabled by the weakly dispersive nature of the Pockels effect used for polarization-insensitive active switching. These results help demonstrate the utility of loop-based quantum memories for quantum networking applications.

A promising approach to long-distance quantum communication involves protocols in which two distant quantum memories become entangled by a central Bell state measurement (BSM) performed on two emitted photons [1,2]. The related process in which two entangled photons emitted from a central source are stored in two distant absorptive quantum memories enables modified protocols that offer advantages in certain quantum network settings [3]. Recent experimental progress in this direction has primarily involved extending earlier demonstrations of single-photon storage in several established quantum memory platforms to the case of storing entangled photons [4–19]. Key results include the storage of entangled photons with MHz bandwidths in atomic ensemble quantum memories [4–9], MHz–GHz bandwidths in solid-state quantum memories [10–18], and THz bandwidths in a diamond quantum memory [19].

In each active approach, the coupling of a photon from a freely propagating mode to the storage mode (typically a collective matter excitation) is accomplished by an externally applied control field that is managed by the user for storage and release of the photons. In addition to bandwidth, key figures of merit include memory efficiency, storage time, accessibility, and output state fidelity. This leads to various trade-offs that can be optimized by different approaches for different applications, and motivates the need for investigations of entanglement storage in other established quantum memory platforms.

Here, we investigate entanglement storage in the "loop-and-switch" based quantum memory platform, which offers large bandwidth and high output state fidelity, but relatively low efficiency and discrete time (rather than continuous) accessibility [20–27]. In this platform, the coupling between the input/output mode and the storage mode (here, switching into and out of a free-space optical storage loop) is implemented by a user-applied dc control field via the Pockels effect. Because this Pockels effect is only weakly dispersive, loop-based memories of this kind can possess ultrawide

bandwidths that can be matched to that of the entangled photons produced by robust and practical conventional spontaneous parametric down-conversion (SPDC) sources (typically $\sim$10 THz). Indeed, broadband Pockels effect based "loop-and-switch" type devices with SPDC sources have recently been used to demonstrate enhanced single-photon production [28–30], measurement-device-independent quantum key distribution [21], switching and storage of Fock states [22,31,32], as well as the generation of multiphoton entangled states [25,26]. Closely related work includes the manipulation of single-photon streams [24,33,34] and continuous-variable entanglement [23] in loop-based systems.

In the present Letter on entangled photon storage with this platform, we use the specific loop-based cyclical quantum memory (CQM) geometry of Ref. [20], and a standard SPDC-based source of polarization-entangled photon pairs [35]. The primary experimental challenge is the nondeterministic nature of the SPDC process, which emits the entangled photons at random (and unknown) times. This precludes triggered switching of the photon pairs into the memories, necessitating random attempts at storage, and, consequently, low overall data rates in the experiment. These data rates are further reduced by the intrinsic loss in the CQMs ($\sim$22% per cycle), which currently hinders long-term storage in our setup. In this proof-of-concept demonstration, we overcome these technical problems to some extent by (1) using pulsed SPDC to restrict the possible emission of a photon pair to well-known time intervals, (2) replacing one of the active CQMs with a much lower loss delay line (fiber spool) serving as a "passive quantum memory" with a fixed storage time, and (3) performing initial alignment and calibration of the system at higher data rates by triggering the active CQM upon detection of the passively stored photon.

Figure 1 provides a conceptual overview of these three ideas, as well as a summary of the relevant timing parameters and detection system used for Bell-test measurements to verify the stored entanglement. The SPDC source is pumped
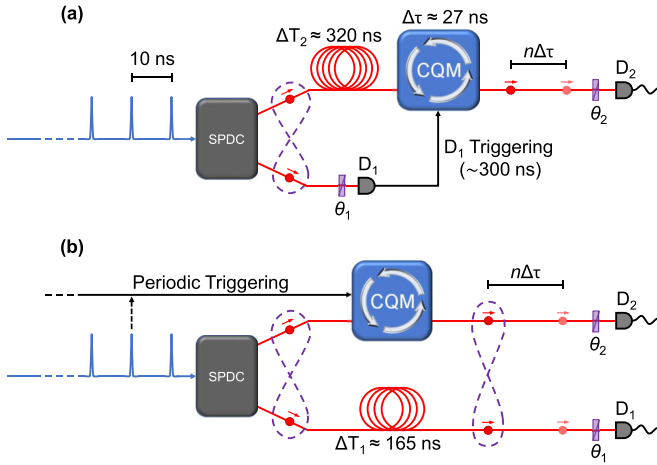
FIG. 1. Conceptual overview of two types of measurements using the broadband pulsed-SPDC and CQM platform: (a) Initial high data rate alignment and calibration measurements in which the CQM is triggered by the detection of photon 1, and (b) lower data rate entanglement storage measurements in which the CQM is periodically triggered. The red circles denote photons, while the dashed purple lines represent entanglement. D_i and θ_i ($i = 1, 2$) are detectors and polarizers used for various Bell-test measurements.

by a 100-MHz pulse train with initial pair production rates on the order of 10 kHz, inferred from the measured coincidence counting rates, single detection rates, and known channel losses and detector efficiencies. This corresponds to an average of one possible pair in the system every 100 μs, while the CQM has a round-trip cycle time of $\Delta\tau \approx 27$ ns and the experiments involve active storage for up to $n = 20$ cycles (∼0.5 μs). Two single-photon detectors (D_1 and D_2) preceded

by polarizers are used to test Bell's inequalities in the system. For the initial testing step shown in Fig. 1(a), the detection of photon 1 is used to trigger the CQM for storage of photon 2, which is then actively released after n cycles. This preliminary test does not represent the storage of entanglement, but allows us to calibrate the setup at higher data rates. Note in Fig. 1(a) that photon 2 is delayed by $\Delta T_2 \sim 320$ ns to compensate for the latency in the detection and CQM switching process [20,28].

Next, in Fig. 1(b), the CQM is periodically triggered by a signal derived from the pump pulse train, which enables the full demonstration of entanglement storage for those cases in which a photon pair is randomly produced at the correct time. In our experiment, we balance the trade-off between a desire for long storage times (i.e., large n) and high data rates (i.e., higher-frequency triggering) to demonstrate entanglement storage for up to $n = 6$ cycles (∼162 ns). Note in Fig. 1(b) that the "passive quantum memory" for photon 1 is fixed at a comparable storage time of $\Delta T_2 \sim 165$ ns. Note also that difficulties associated with failed storage attempts and loss in the CQM are largely overcome by the postselective nature of the Bell tests used to study the ability of the system to store entanglement; only attempts in which both D_1 and D_2 register a photon are recorded [36].

Figure 2 shows a schematic of the complete experimental setup. For convenience, the figure highlights five different shaded regions corresponding to the key aspects of the experiment. The SPDC source consists of a 0.7-mm-thick beta barium borate (BBO) crystal pumped by a 100-MHz pulse train at 390 nm derived from the frequency-doubled output of a mode-locked fiber laser (Menlo Systems C-Fiber 780; pulse widths ∼100 fs), and produces photon pairs with a central wavelengths of 780 nm. Interference filters with a bandwidth
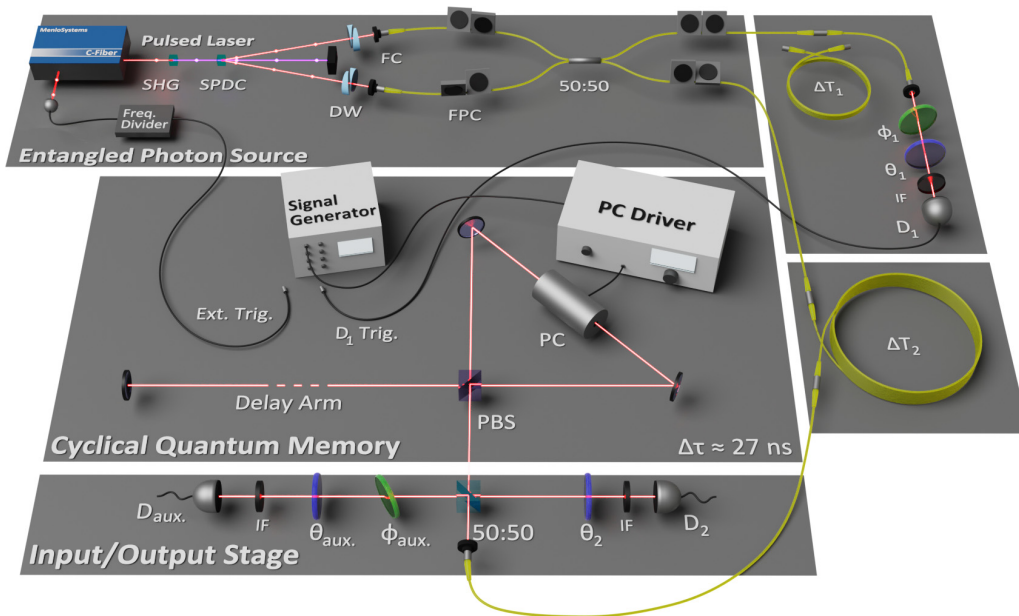

FIG. 2. Schematic of the experimental apparatus. Translatable delay wedge prisms (DW) are used to adjust the timing of the down-converted photons, and a 50:50 fiber coupler with fiber polarization controllers (FPC) is used to realize entangled states of the form $|\psi^-\rangle = 1/\sqrt{2}(|H_1 V_2\rangle - e^{i\phi}|V_1 H_2\rangle)$ using the Shih-Alley technique [35]. Phase shifters ϕ_{aux} and ϕ_1 are used to compensate for the combination of ϕ and any net birefringent phase shifts in fiber spools ΔT_1, ΔT_2, and the CQM itself for the "before storage" and "after storage" Bell inequality tests. (SHG: second-harmonic generation; FC: fiber coupling lenses; IF: 25-nm bandwidth interference filters.)

of 25 nm are used to define the photon bandwidths ($\sim$10 THz). We use type-I noncollinear SPDC and the Shih-Alley (SA) technique at a 50:50 beam splitter [35] to postselect entangled states of the form $|\psi^-\rangle = 1/\sqrt{2}(|H_1V_2\rangle - |V_1H_2\rangle)$, where H and V denote horizontally and vertically polarized photons and the subscripts correspond to output channels 1 and 2. Photon 1 is detected in the direct output of the SA beam splitter, while photon 2 is sent to the CQM which, in our laboratory, is located on a second optical table roughly 6 m from the source.

Complete details of the operational technique of the loop-based CQM are provided in Ref. [20]. To summarize, it consists of a high-speed Pockels cell (PC) placed in a Sagnac-like interferometer formed by a polarizing beam splitter (PBS), two broadband mirrors, and a lengthy "out and back" delay arm. Incident photons are delocalized into two counterpropagating H and V polarization components that are repeatedly "flipped" (i.e., $H \leftrightarrow V$) each time they pass through the PC in the "on" state. This leads to a self-cancellation effect for phase shift errors due to birefringence in the CQM for photons stored for an even number n of cycles. In addition, bit flip errors (imperfect polarization rotations) are ejected from the CQM geometry at incorrect times, contributing only to overall loss.

We use a lithium tantalate (LTA) multicrystal-based PC operated in a transverse configuration (ConOptics model 360-80, with 25D driver), with a half-wave voltage of only 140 V at 780 nm, and rise and fall times (i.e., switching times) of $\sim$15 ns, which are safely shorter than the 27 ns cycle time of the CQM. The user actively stores the incident photon, and releases it after a chosen value of n cycles, by simply switching the PC between its on and off states at the appropriate times.

As shown in Fig. 2, the PC driver is activated by a short-pulse signal generator that is triggered by either (1) the detection of a photon in D_1 for the initial tests of Fig. 1(a), or (2) a periodic signal derived by frequency division of a 100 MHz synchronization signal from the mode-locked laser for the main entanglement storage experiments of Fig. 1(b). In addition, the delays ΔT_1 and ΔT_2 required for these two types of experiments are formed by fiber spools that can be inserted and removed as needed.

A key 50:50 beam splitter is inserted in the CQM input channel to reflect the CQM output to the second Bell-test detector D_2. While this reduces the CQM overall efficiency to a maximum value of 25% in this proof-of-concept experiment, it also provides a valuable auxiliary detection channel that can be used *in situ* for comparative Bell tests: Bell tests "before storage" use correlations between detectors D_1 and D_{aux}, while Bell tests "after storage" are performed with D_1 and D_2. We note that this efficiency limitation can be overcome by replacing the 50:50 beam splitter with a high-quality optical circulator or polarization to time-bin transduction methods in the loop-based memory platform [21,25,27].

Additional tests of the PC with various lasers confirmed that with the half-wave voltage set for perfect $90°$ polarization rotation ("flipping") of 780 nm light, a wavelength range greater than 25 nm (near 780 nm) would be "flipped" with greater than 95% fidelity due to the weakly dispersive birefringence of the Pockels effect in our system. Combined with very broadband CQM mirror reflectivities ($R > 98\%$ for H
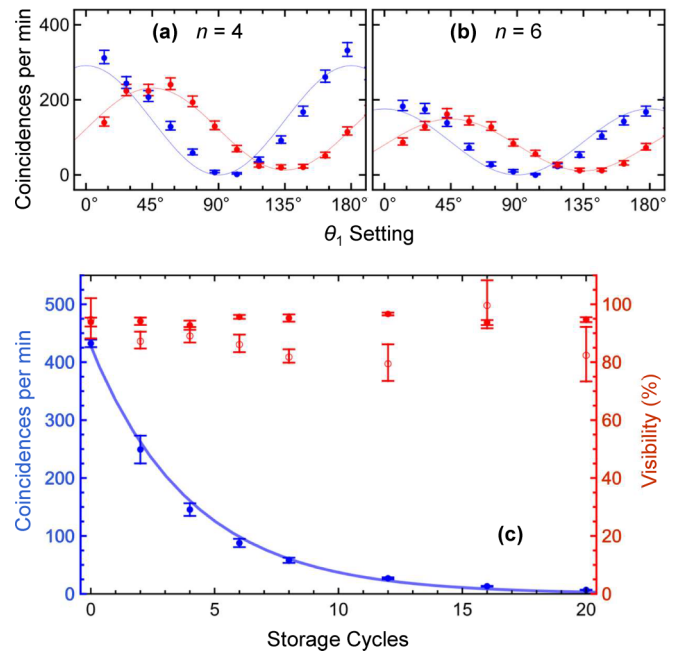

FIG. 3. Summary of experimental results from the high data rate test and alignment measurements: (a) Heralded output state polarization measurements for storage of $n = 4$ cycles. Blue data correspond to θ_2 fixed at $0°$, while red data correspond to $\theta_2 = 45°$; (b) analogous results for $n = 6$ cycles; (c) summary of extracted average coincidence rates (blue data) and visibilities in the $-45°/45°$ basis from before storage runs (red data, open circles) and after storage runs (red data, solid circles) for various storage times up to $n = 20$ cycles (540 ns).

and V components over 750–1100 nm), this enables the CQM to serve as a high-speed broadband optical quantum memory device.

Figure 3 shows a summary of calibration data using the arrangement of Fig. 1(a). While this arrangement does not demonstrate the storage of entanglement, we perform various measurements using the same polarizer settings needed to characterize the expected performance of the system for subsequent Bell tests. Figures 3(a) and 3(b) show plots of the coincidence counting rates between D_1 and D_2 as a function of θ_1 after heralded storage of photon 2 for $n = 4$ and $n = 6$ cycles, respectively, for the cases of θ_2 fixed at $0°$ (blue data) and $45°$ (red data). The sinusoidal fits to the data are then used to extract the visibilities from the red curves (a measure of output state polarization fidelity) and the average counting rates from the blue curves (a measure of loss during storage). Analogous data sets (not shown) were taken for storage up to $n = 20$ cycles, as well as for the before storage case using coincidence counts between detectors D_1 and D_{aux}. These data sets were all taken in rapid succession with minimal adjustments to the setup in order to study the system's performance as a function of n. Figure 3(c) summarizes these data and provides two main results: An exponential fit to the average count rate (blue data) shows a CQM loss of roughly 22% per cycle [37], while the after storage visibility (red data, solid circles) shows essentially no degradation with increasing storage time.
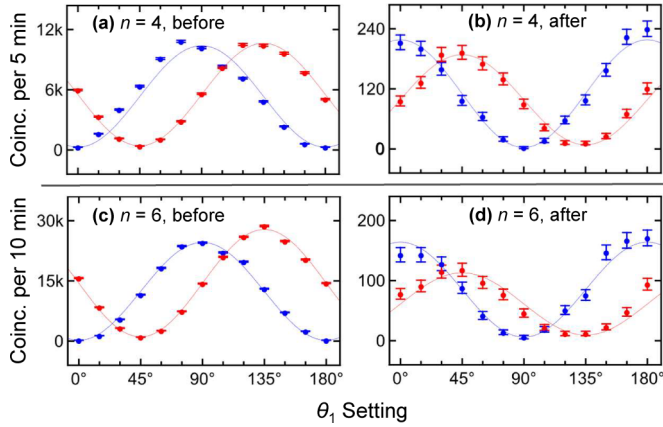
FIG. 4. Summary of experimental results demonstrating entanglement storage: (a) and (b) show before storage and after storage polarization correlations for the case of $n = 4$ cycles, with blue (red) data corresponding to θ_2 fixed at $0°$ ($45°$). The sinusoidal data in (b) are shifted by $90°$ due to the intrinsic bit flipping in the CQM. (c) and (d) show analogous results for the case of $n = 6$ cycles. The high visibilities of the fits to the data violate the CHSH form of Bell's inequality [38] and demonstrate the ability to store entanglement in the SPDC and loop-based quantum memory platform.

These preliminary loss and visibility results of Fig. 3(c) provide an expectation of being able to violate Bell's inequality after storing entanglement using the arrangement of Fig. 1(b) for increasingly long storage times, until the overall loss in the CQM drives the signal-to-noise ratio in the system down to an unmanageable level. This leads to the main results of the Letter illustrated in Fig. 4, which shows examples of this entanglement storage for the case of $n = 4$ and 6 cycles.

Figures 4(a) and 4(b) correspond to the before storage and after storage coincidence count data for the case of $n = 4$ cycles. The experimental data show the expected $\sin^2(\theta_1 - \theta_2)$ signature of the $|\psi^-\rangle$ Bell state, with before storage measured visibilities of $(95 \pm 3)\%$ in the H/V basis and $(92 \pm 1)\%$ in the $-45°/45°$ basis, and corresponding after storage visibilities of $(97 \pm 1)\%$ and $(91 \pm 4)\%$. As is well known, combined visibilities greater than 71% in these experimental situations are sufficient for a violation of the Clauser-Horne-Shimony-Holt (CHSH) form of Bell's inequality subject to certain reasonable assumptions [36], and here correspond to Bell parameter values of $S = 2.64 \pm 0.04$ before storage, and $S = 2.66 \pm 0.06$ after storage [38]. In this proof-of-concept experiment, these $S > 2$ parameter values provide a demonstration of the ability to store and maintain polarization entanglement in the loop-based quantum memory platform.

Figures 4(c) and 4(d) show analogous results for the case of $n = 6$ cycles. Here, the before storage measured visibilities are $(98 \pm 1)\%$ in the H/V basis and $(93 \pm 1)\%$ in the $-45°/45°$ basis, with corresponding after storage visibilities of $(93 \pm 3)\%$ and $(85 \pm 7)\%$. These visibilities correspond to Bell parameter values of $S = 2.69 \pm 0.02$ before storage and $S = 2.52 \pm 0.11$ after storage, once again demonstrating successful entanglement storage. We suspect the slightly lower S value in the after storage case was primarily due to small misalignments that occurred in the CQM between data runs, as well as the reduction in overall data rates which

necessitated longer collection times and thus increased experimental instabilities during the $n = 6$ cycle run. As a technical point of interest in the experiment, the longer storage times associated with increasing values of n require larger divisions of the 100-MHz periodic CQM triggering signal to prevent accidental "on/off" state overlap in the PC during storage. These less frequent attempts at storage corresponded to significant data rate reductions for large n, which are then further reduced by the accumulating intrinsic CQM loss of 22% per cycle. An accurately calibrated observation of these count rate reductions is not possible in Fig. 4 due to small changes in the experimental conditions that occurred between these nonsequential data runs. Nonetheless, further increases in these two types of data rate reduction mechanisms for increasing n prevented realistic attempts at entanglement storage for, say, 20 cycles in our current proof-of-concept type setup.

In summary, we have demonstrated the storage of entangled photons with ~10 THz bandwidths from a conventional SPDC source using one active broadband loop-based quantum memory device, and a second "passive quantum memory" formed by a simple delay line, in analogy with earlier entanglement storage demonstrations using other quantum memory platforms [5,10,11,13–15,19]. The experimental results represent a demonstration of a rudimentary entanglement distribution protocol, in which one member of an entangled pair is delivered to a location A at a fixed time, while the other is delivered to a second distant location B at an arbitrarily chosen time.

The broadband nature of the loop-based memory platform helps overcome the notorious "bandwidth matching" problem associated with using traditional broadband SPDC entangled photon sources and narrowband atomic quantum memories [5]. However, it is important to note that the lack of an intrinsic optical nonlinearity in the loop-based platform represents a drawback for multinode quantum repeater-type applications in which a single node acts as both a memory and a quantum processor [39]. For these more challenging protocols, supplementing the loop-based memory with additional probabilistic techniques from the linear optics quantum computing paradigm would be required [40].

The primary limitation in this proof-of-concept experiment was the use of randomly produced entangled photon pairs, which essentially necessitated random attempts at storage and thus low overall data rates. For future applications, these difficulties can be completely overcome by the use of heralded entangled pairs that can be produced by combining several random SPDC sources [41–44]. We note that for more demanding applications, these same heralded SPDC sources can, in principle, be converted to "on-demand" entanglement sources by using two loop-based memories and some of the techniques demonstrated in the present Letter [42]. Consequently, near-term implementations of various multiphoton quantum networking and entanglement distribution protocols could benefit from the use of robust broadband SPDC sources and ultrabroadband loop-based memories, and the proof-of-concept experimental results presented here represent a tangible step in that direction.

[1] C. Simon and W. T. M. Irvine, Robust long-distance entanglement and a loophole-free Bell test with ions and photons, Phys. Rev. Lett. **91**, 110405 (2003).

[2] N. Sangouard, C. Simon, H. de Riedmatten, and N. Gisin, Quantum repeaters based on atomic ensembles and linear optics, Rev. Mod. Phys. **83**, 33 (2011).

[3] C. Jones, D. Kim, M. Rakher, P. Kwiat, and T. Ladd, Design and analysis of communication protocols for quantum repeater networks, New J. Phys. **18**, 083015 (2016).

[4] K. S. Choi, H. Deng, J. Laurat, and H. J. Kimble, Mapping photonic entanglement into and out of a quantum memory, Nature (London) **452**, 67 (2008).

[5] K. Akiba, K. Kashiwagi, M. Arikawa, and M. Kozuma, Storage and retrieval of nonclassical photon pairs and conditional single photons generated by the parametric down-conversion process, New J. Phys. **11**, 013049 (2009).

[6] H. Zhang, X.-M. Jin, J. Yang, H.-N. Dai, S.-J. Yang, T.-M. Zhao, J. Rui, Y. He, X. Jiang, F. Yang, G.-S. Pan, Z.-S. Yuan, Y. Deng, Z.-B. Chen, X.-H. Bao, S. Chen, B. Zhao, and J.-W. Pan, Preparation and storage of frequency-uncorrelated entangled photons from cavity-enhanced spontaneous parametric down-conversion, Nat. Photon. **5**, 628 (2011).

[7] H.-N. Dai, H. Zhang, S.-J. Yang, T.-M. Zhao, J. Rui, Y.-J. Deng, L. Li, N.-L. Liu, S. Chen, X.-H. Bao, X.-M. Jin, B. Zhao, and J.-W. Pan, Holographic storage of biphoton entanglement, Phys. Rev. Lett. **108**, 210501 (2012).

[8] D.-S. Ding, W. Zhang, Z.-Y. Zhou, S. Shi, B.-S. Shi, and G.-C. Guo, Raman quantum memory of photonic polarized entanglement, Nat. Photon. **9**, 332 (2015).

[9] M. Cao, F. Hoffet, S. Qiu, A. S. Sheremet, and J. Laurat, Efficient reversible entanglement transfer between light and quantum memories, Optica **7**, 1440 (2020).

[10] C. Clausen, I. Usmani, F. Bussières, N. Sangouard, M. Afzelius, H. de Riedmatten, and N. Gisin, Quantum storage of photonic entanglement in a crystal, Nature (London) **469**, 508 (2011).

[11] E. Saglamyurek, N. Sinclair, J. Jin, J. A. Slater, D. Oblak, F. Bussières, M. George, R. Ricken, W. Sohler, and W. Tittel, Broadband waveguide quantum memory for entangled photons, Nature (London) **469**, 512 (2011).

[12] I. Usmani, C. Clausen, F. Bussières, N. Sangouard, M. Afzelius, and N. Gisin, Heralded quantum entanglement between two crystals, Nat. Photon. **6**, 234 (2012).

[13] Félix Bussières, C. Clausen, A. Tiranov, B. Korzh, V. B. Verma, S. W. Nam, F. Marsili, A. Ferrier, P. Goldner, H. Herrmann, C. Silberhorn, W. Sohler, M. Afzelius, and N. Gisin, Quantum teleportation from a telecom-wavelength photon to a solid-state quantum memory, Nat. Photon. **8**, 775 (2014).

[14] Z.-Q. Zhou, Y.-L. Hua, X. Liu, G. Chen, J.-S. Xu, Y.-J. Han, C.-F. Li, and G.-C. Guo, Quantum storage of three-dimensional orbital-angular-momentum entanglement in a crystal, Phys. Rev. Lett. **115**, 070502 (2015).

[15] E. Saglamyurek, J. Jin, V. B. Verma, M. D. Shaw, F. Marsili, S. W. Nam, D. Oblak, and W. Tittel, Quantum storage of entangled telecom-wavelength photons in an erbium-doped optical fibre, Nat. Photon. **9**, 83 (2015).

[16] M. li Grimau Puigibert, M. F. Askarani, J. H. Davidson, V. B. Verma, M. D. Shaw, S. W. Nam, T. Lutz, G. C. Amaral, D. Oblak, and W. Tittel, Entanglement and nonlocality between disparate solid-state quantum memories mediated by photons, Phys. Rev. Res. **2**, 013039 (2020).

[17] J. V. Rakonjac, D. Lago-Rivera, A. Seri, M. Mazzera, S. Grandi, and H. de Riedmatten, Entanglement between a telecom photon and an on-demand multimode solid-state quantum memory, Phys. Rev. Lett. **127**, 210502 (2021).

[18] X. Liu, J. Hu, Z.-F. Li, X. Li, P.-Y. Li, P.-J. Liang, Z.-Q. Zhou, C.-F. Li, and G.-C. Guo, Heralded entanglement distribution between two absorptive quantum memories, Nature (London) **594**, 41 (2021).

[19] K. A. G. Fisher, D. G. England, J.-P. W. MacLean, P. J. Bustard, K. Heshami, K. J. Resch, and B. J. Sussman, Storage of polarization-entangled THz-bandwidth photons in a diamond quantum memory, Phys. Rev. A **96**, 012324 (2017).

[20] T. B. Pittman and J. D. Franson, Cyclical quantum memory for photonic qubits, Phys. Rev. A **66**, 062302 (2002).

[21] F. Kaneda, F. Xu, J. Chapman, and P. G. Kwiat, Quantum-memory-assisted multi-photon generation for efficient quantum information processing, Optica **4**, 1034 (2017).

[22] M. Bouillard, G. Boucher, J. Ferrer Ortas, B. Pointard, and R. Tualle-Brouri, Quantum storage of single-photon and two-photon Fock states with an all-optical quantum memory, Phys. Rev. Lett. **122**, 210501 (2019).

[23] S. Takeda, K. Takase, and A. Furusawa, On-demand photonic entanglement synthesizer, Sci. Adv. **5**, eaaw4530 (2019).

[24] X.-L. Pang, A.-L. Yang, J.-P. Dou, H. Li, C.-N. Zhang, E. Poem, D. J. Saunders, H. Tang, J. Nunn, I. A. Walmsley, and X.-M. Jin, A hybrid quantum memory-enabled network at room temperature, Sci. Adv. **6**, eaax1425 (2020).

[25] E. Meyer-Scott, N. Prasannan, I. Dhand, C. Eigner, V. Quiring, S. Barkhofen, B. Brecht, M. B. Plenio, and C. Silberhorn, Scalable generation of multiphoton entangled states by active feed-forward and multiplexing, Phys. Rev. Lett. **129**, 150501 (2022).

[26] Z. Hou, J.-F. Tang, C.-J. Huang, Y.-F. Huang, G.-Y. Xiang, C.-F. Li, and G.-C. Guo, Entangled-state time multiplexing for multi-photon entanglement generation, Phys. Rev. Appl. **19**, L011002 (2023).

[27] N. Arnold, M. Victora, M. Goggin, and P. G. Kwiat, Free-space photonic quantum memory, in *Quantum Computing, Communication, and Simulation III*, edited by P. R. Hemmer and A. L. Migdall (SPIE, San Francisco, 2023), p. 10.

[28] T. B. Pittman, B. C. Jacobs, and J. D. Franson, Single photons on pseudodemand from stored parametric down-conversion, Phys. Rev. A **66**, 042303 (2002).

[29] F. Kaneda, B. G. Christensen, J. J. Wong, H. S. Park, K. T. McCusker, and P. G. Kwiat, Time-multiplexed heralded single-photon source, Optica **2**, 1010 (2015).

[30] F. Kaneda and P. G. Kwiat, High-efficiency single-photon generation via large-scale active time multiplexing, Sci. Adv. **5**, eaaw8586 (2019).

[31] A. Alarcón, P. González, J. Cariñe, G. Lima, and G. B. Xavier, Polarization-independent single-photon switch based on a fiber-optical Sagnac interferometer for quantum communication networks, Opt. Express **28**, 33731 (2020).

[32] A. Z. Leger, S. Gambhir, J. Légère, and D. R. Hamel, Amplification of cascaded down-conversion by reusing photons with a switchable cavity, Phys. Rev. Res. **5**, 023131 (2023).

[33] D. Istrati, Y. Pilnyak, J. C. Loredo, C. Antón, N. Somaschi, P. Hilaire, H. Ollivier, M. Esmann, L. Cohen, L. Vidro, C. Millet, A. Lemaître, I. Sagnes, A. Harouri, L. Lanco, P. Senellart,

and H. S. Eisenberg, Sequential generation of linear cluster states from a single photon emitter, Nat. Commun. **11**, 5501 (2020).

[34] K. Makino, Y. Hashimoto, J.-I. Yoshikawa, H. Ohdan, T. Toyama, P. van Loock, and A. Furusawa, Synchronization of optical photons for quantum information processing, Sci. Adv. **2**, e1501772 (2016).

[35] Y. H. Shih and C. O. Alley, New Type of Einstein-Podolsky-Rosen-Bohm experiment using pairs of light quanta produced by optical parametric down conversion, Phys. Rev. Lett. **61**, 2921 (1988).

[36] J. F. Clauser, M. A. Horne, A. Shimony, and R. A. Holt, Proposed experiment to test local hidden-variable theories, Phys. Rev. Lett. **23**, 880 (1969).

[37] The loss budget consists of 10% loss in the Pockels cell, 5% transmission/reflection losses at the PBS and mirrors, and the remaining 7% due to small misalignments and imperfect polarization rotations.

[38] W. Tittel, J. Brendel, N. Gisin, and H. Zbinden, Long-distance Bell-type tests using energy-time entangled photons, Phys. Rev. A **59**, 4150 (1999).

[39] V. Krutyanskiy, M. Canteri, M. Meraner, J. Bate, V. Krcmarsky, J. Schupp, N. Sangouard, and B. P. Lanyon, Telecom-wavelength quantum repeater node based on a trapped-ion processor, Phys. Rev. Lett. **130**, 213601 (2023).

[40] E. Knill, R. Laflamme, and G. J. Milburn, A scheme for efficient quantum computation with linear optics, Nature (London) **409**, 46 (2001).

[41] C. Śliwa and K. Banaszek, Conditional preparation of maximal polarization entanglement, Phys. Rev. A **67**, 030101(R) (2003).

[42] T. Pittman, M. Donegan, M. Fitch, B. Jacobs, J. Franson, P. Kok, H. Lee, and J. Dowling, Heralded two-photon entanglement from probabilistic quantum logic operations on multiple parametric down-conversion sources, IEEE J. Sel. Top. Quantum Electron. **9**, 1478 (2003).

[43] C. Wagenknecht, C.-M. Li, A. Reingruber, X.-H. Bao, A. Goebel, Y.-A. Chen, Q. Zhang, K. Chen, and J.-W. Pan, Experimental demonstration of a heralded entanglement source, Nat. Photon. **4**, 549 (2010).

[44] S. Barz, G. Cronenberg, A. Zeilinger, and P. Walther, Heralded generation of entangled photon pairs, Nat. Photon. **4**, 553 (2010).